ADVANCED MATERIALS

Supporting Information

for *Adv. Mater.*, DOI: 10.1002/adma.201803151

Coupling Interface Constructions of $MoS_2/Fe_5Ni_4S_8$ Heterostructures for Efficient Electrochemical Water Splitting

Yi Wu, Fan Li, Wenlong Chen, Qian Xiang, Yanling Ma, Hong Zhu, Peng Tao, Chengyi Song, Wen Shang, Tao Deng, and Jianbo Wu**

Supporting Information

Coupling Interface Constructions of $MoS_2/Fe_5Ni_4S_8$ Heterostructures for Efficient Electrochemical Water Splitting

Yi Wu[a], Fan Li[a], Wenlong Chen[a], Qian Xiang[a], Yanling Ma[a], Hong Zhu[a,b,c*], Peng Tao[a], Chengyi Song[a], Wen Shang[a], Tao Deng[a], Jianbo Wu[a,c*]

M.S. Y. Wu, Dr. F. Li, Dr. W. Chen, Dr. Q. Xiang, Dr. Y. Ma, Prof. H. Zhu, Prof. P. Tao, Prof. C. Song, Prof. W. Shang, Prof. T. Deng, Prof. J. Wu
State Key Laboratory of Metal Matrix Composites
School of Materials Science and Engineering
Shanghai Jiao Tong University, 800 Dongchuan Road, Shanghai, 200240, P. R.
E-mail: jianbowu@sjtu.edu.cn; hong.zhu@sjtu.edu.cn
Prof. H. Zhu
University of Michigan – Shanghai Jiao Tong University Joint Institute
Shanghai Jiao Tong University, 800 Dongchuan Road, Shanghai, 200240, P. R.
Prof. H. Zhu, Prof. J. Wu
Materials Genome Initiative Center
Shanghai Jiao Tong University, 800 Dongchuan Road, Shanghai, 200240, P. R.

Experimental section

Materials

FeNi foam with 1 mm thickness (50% Fe, 50% Ni) and FeNi foil (50% Fe, 50% Ni) with 0.3 mm (Shanghai Yilong Experimental Equipment Co. Ltd.). Molybdenum trioxide powder (MoO_3, M104353, Aladdin), sulfur powder (S, 99.5%, Alfa), 300 nm SiO_2/Si plates (SiBranch intern. Com. Ltd.), platinum (Pt/C, nominally 20% on carbon black, Alfa), iridium oxide (IrO_2, 99.99%, Alfa), all chemicals were used as received without further purification if not mentioned.

Synthesize MoS_2 on FeNi foam

All reactions were taken place in a three-temperature-zone furnace (GSL-1700X-Ⅲ) under ambient pressure as shown in Figure S1. Firstly, 300 nm SiO_2/Si plate was cut into 1 mm * 1 mm and FeNi foam was cut into 1.2 mm * 1.5 mm. FeNi foam and SiO_2/Si were sequentially sonicated in acetone, ethanol, 0.5 M HCl and deionized water, respectively. Then, 5 mg MoO_3 powders were placed carefully onto the 1 mm * 1 mm SiO_2/Si plate, which was transferred into a quartz boat. The 0.8 mm * 0.8 mm SiO_2/Si was put face-up and the FeNi foam was put over the SiO_2/Si. Then, the quartz boat was moved in the center of the central zone of the furnace and another quartz boat with 300 mg sulfur was put in the center of the entrant zone. For a contrast of distance between sulfur and MoO_3, one more quartz boat with the same way treated SiO_2/Si plates was put in the center of the terminate zone. Before reaction, 500 sccm nitrogen was introduced to purge the ambient gas for 30 min. Then, the gas flow was changed to 50 sccm, meanwhile, the second and third zone were heated up to 650 ^{o}C within 30 minutes. Subsequently, the first zone was heated to 110 ^{o}C immediately. After reaction for 10 minutes, the system was naturally cooling down and the MoS_2/FNS/FeNi foam was obtained.

Synthesize MoS_2 on SiO_2/Si substrate

300 nm SiO_2/Si was used as a substrate to grow MoS_2 NSs. Cut into 0.8 mm * 0.8 mm and 1.2 mm * 1.2 mm, the bigger SiO_2/Si plate was placed face-down up the MoO_3 powder coated on the smaller SiO_2/Si plate in the furnace. And the rest treatments were prepared just like the above synthesis on FeNi foam. The triangular MoS_2 can be easily observed on the 1.2 mm * 1.2 mm SiO_2/Si by optical microscope owning to the optical contrast.

Synthesize MoS_2 on other substrates

FeNi foil, fluorine-doped tin oxide (FTO) were used as substrates to grow MoS_2 NSs. All substrates were cut into 1.2 mm * 1.5 mm and placed face-down up the MoO_3 powder coated on 1 mm * 1 mm SiO_2/Si plate in the furnace, respectively. And the rest treatments were prepared just like the above synthesis on SiO_2/Si.

Synthesize $Fe_5Ni_4S_8$ (FNS)

FeNi foam and FeNi foil substrate were used, the procedure was conducted as above, except there was no MoO_3 source.

Material characterization

The optical images were observed by the optical microscope (UCMOS 14000KPA, TOUPCAM). The morphology was characterized by a field-emission SEM (JSM-7800, JEOL) operating at 5 kV and high resolution TEM (JSM-2100F, JEOL) operating at 200 kV. High angle annular dark field scanning TEM (HAADF-STEM) and energy dispersive X-ray (EDX) elements mappings were taking using a JEOL JEM-ARM200F microscope operated at 200 KV. The X-ray diffraction patterns were recorded using an X-ray diffractometer (LabX XRD-6100, Shimadzu) from 10^o to 80^o at a scan rate of 10 ^{o}/min and Cu Kα radiation resource. The Raman spectra were obtained using by Dispersive Raman spectroscopy Senterra R200-L. The X-ray photoelectron spectroscopy (XPS) was carried out by the AXIS Ultra DLD equipment and the binding energy of C 1s peak at 284.8 eV was taken as an internal standard. The mass loading was confirmed by the iCAP6300 (ICP).

Electrochemical test

All electrochemical tests were performed at room temperature. The HER performance was evaluated in Ar-saturated 1.0 M KOH solution using linear scan voltammetry (LSV) and Amperometric i-t mode on an electrochemical workstation (CHI760E, CHI instrument and SP-200, Bio-Logic) with the three-electrode configuration on a stirring platform. The stirring rate was set 300 r/min to diffuse the bubbles quickly. The reference electrode was reversible hydrogen electrode (RHE, HydroFlex, Gaskate), the counter electrode was a graphite rod (The counter electrode may dissolve and the process may have an influence on the tested performance. Thus, the active platinum should not be considered as the ideal counter electrode) and the working electrode was our target material clipped, prepared by blocking off one side of the substrate with an insulating epoxy. The typical geometrical area of the working electrode is the total proportion of substrate, detached by the clamp's area. The 1 M KOH electrolyte was bubbled by Ar for 30 min, followed by LSV test at a scan rate of 1 mV/s from

0.1 V to -0.6 V. For comparison, Pt/C (20%, Alfa) was loaded on FeNi foam with 0.8 mg/cm^2. All current density values are normalized with respect to the geometrical surface area of the working electrode. The stability measurement was operated at the potential@10 mA/cm^2 for 10 h by Amperometric i-t mode. All LSV curves are iR corrected by the following equation:

$$E_c=E_m-iR_s \quad (1)$$

Where E_c is the iR-corrected potential, E_m is the measured potential, i is the current and R_s is the uncompensated circuit resistance extracted from the CHI 760E (In this work, the solution resistances are ~1 Ω for FeNi-based materials and 15.8 Ω for FTO/MoS_2).

The OER test was conducted in O_2-saturated 1.0M KOH solution by cyclic voltammetry (CV) test at a scan rate of 1 mV/s from 1 V to 1.8 V for 40 segments. The configurations are the same as that of HER measurement, except the counter electrode become a pure Pt wire. Tafel curves were obtained by the backward CV curves. For comparison, IrO_2 was loaded on FeNi foam with 0.5 mg/cm^2. The stability test of LSV was conducted at the potential@10 mA/cm^2 for 10 h in the amperometric i-t mode.

The electrochemical impedance spectroscopy (EIS) measurements were carried out in the same configuration at η= 250 mV from 100 KHz to 0.01 Hz.

Computational details and models

The theoretical calculations were performed at the level of density functional theory (DFT) using the Vienna ab-initio simulation package (VASP) [1]. The core and valence electrons were represented by the projector augmented wave (PAW) method and plane–wave basis functions with a kinetic energy cut-off of 520 eV [2]. The generalized gradient approximation (GGA) with the Perdew-Burke-Ernzerhof (PBE) exchange-correlation functional was used in the calculations [3]. A six-layer of MoS_2 (103) was chosen as the surface slab supercell on the basis of high resolution transmission electron microscope (HRTEM) results, separated by 15.0 Å thick vacuum layer. According to the XRD and HRTEM, another surface slab supercell should be $Fe_5Ni_4S_8$ (422), whose phase prototype is Co_9S_8 (Figure S13) and there is a chance of 5/9 for Fe and 4/9 for Ni in the position of Co. A six-layer of Fe_9S_8 (422) and a six-layer of Ni_9S_8 (422) were chosen as the surface slab supercell to decrease the complexity of calculation. To investigate the effect of MoS_2/$Fe_5Ni_4S_8$ heterostructures, we doped MoS_2 (103) with Fe and Ni, while doping Fe_9S_8 (422) and Ni_9S_8 (422) with Mo. The energy convergence criterion is 0.00005 eV/atom for electronic minimization steps.

To elucidate the origin of the high reactivity of HER and OER, adsorption energy for H on MoS_2 (103) and Fe, Ni-MoS_2 (103) and OH on Fe_9S_8 (422), Ni_9S_8 (422), Mo-Fe_9S_8 (422) and

$Mo\text{-}Ni_9S_8$ (422) were calculated. A preferred consideration about the adsorption sites of H is applied, including the top site on S, while the adsorption sites of OH tend to adsorb on top and bridge site on Mo, Fe or Ni.4 The selection of each adsorption energy was arranged by the strongest one. And the adsorption energy can be achieved as follows:

$$\Delta G_{ads(H)} = E_{s\text{-}H} - E_s - E_H \quad (2)$$

$$\Delta G_{ads(OH)} = E_{s\text{-}OH} - E_s - E_{OH} \quad (3)$$

Where $\Delta G_{ads(H)}$ and $\Delta G_{ads(OH)}$ is the adsorption energy of H and OH, respectively. $E_{s\text{-}H}$ and $E_{s\text{-}OH}$ is their individual energy of the catalyst with the adsorbate, H and OH. E_s is the energy of the catalyst without the adsorbate. While E_H and E_{OH} is the energy of H and OH.

Supplementary Figures:

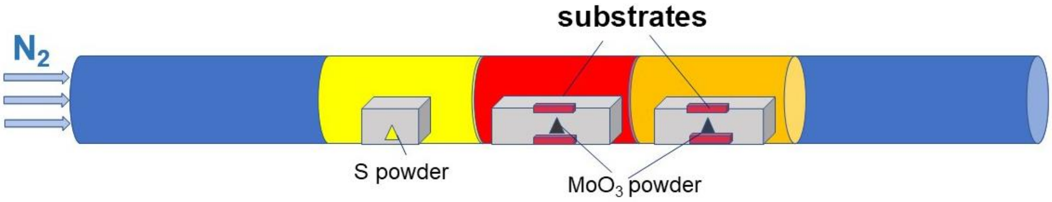

Figure S1. Schematism of CVD-grown MoS_2 on specific substrates.

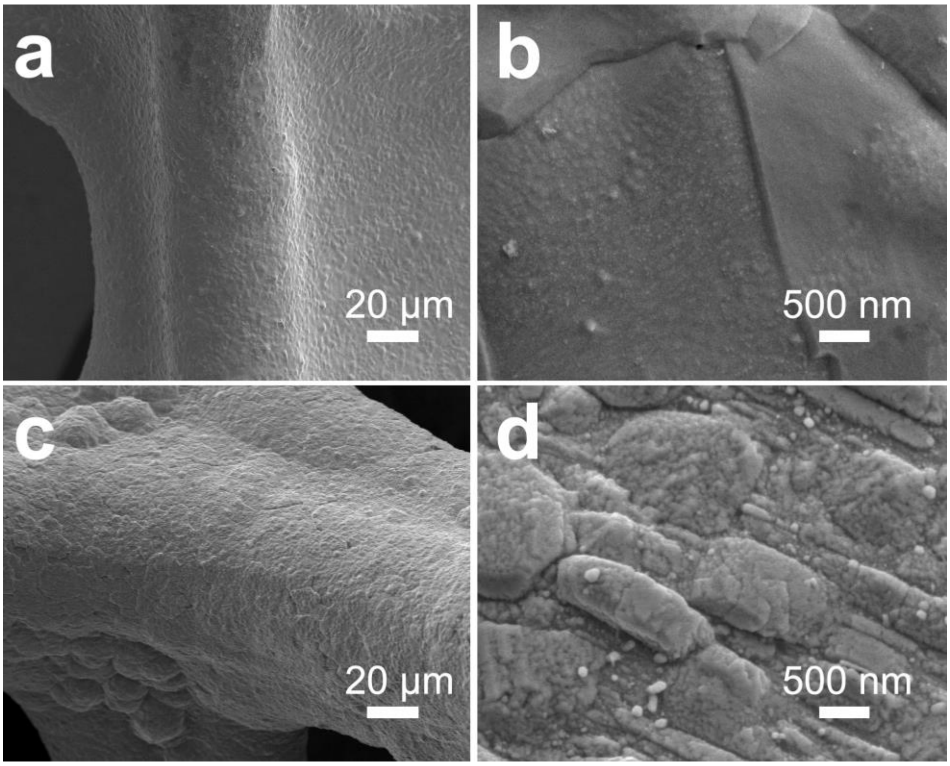

Figure S2. SEM of pure FeNi foam and FNS/FeNi foam in a flow rate of 50 sccm of N_2 at 650 ^oC for 10 min. (a, b) pure FeNi foam, (c, d) FNS/FeNi foam.

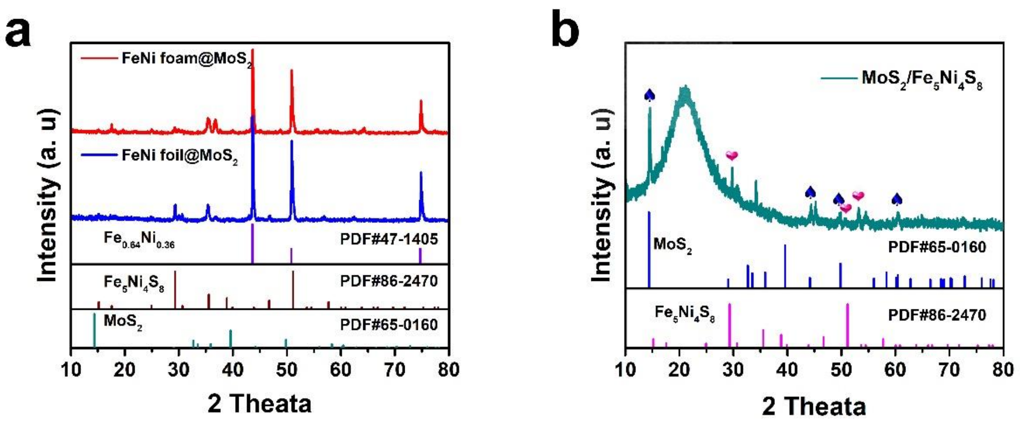

Figure S3. XRD patterns of MoS_2/FNS/FeNi. (a) the MoS_2/FNS sample on FeNi substrates, (b) freestanding MoS_2/FNS powder. As FeNi substrate signal of bulk samples is much higher than MoS_2 and FNS, sonication has been carried out to collect MoS_2/FNS powder. The peak around 20^o in (b) is caused by the amorphous glass substrate of XRD measurement.

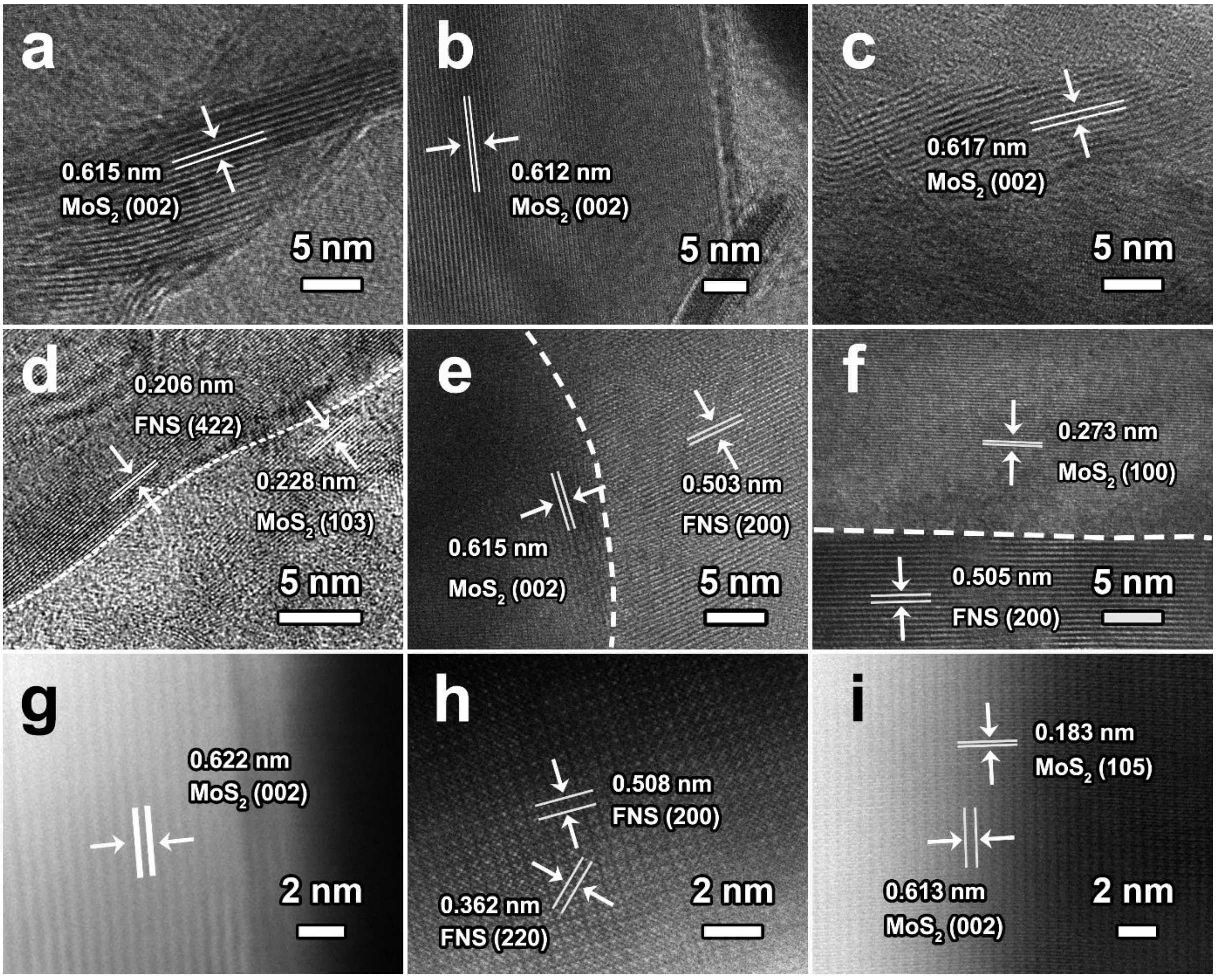

Figure S4. HR-TEM and HAADF-STEM images of MoS_2/FNS structures. (a-c) HR-TEM images of MoS_2; (b-f) HR-TEM of MoS_2/FNS interfaces; (g-i) Atomic resolution HAADF-STEM images of MoS_2 and FNS. The white dashed lines in d-f highlight the interfaces.

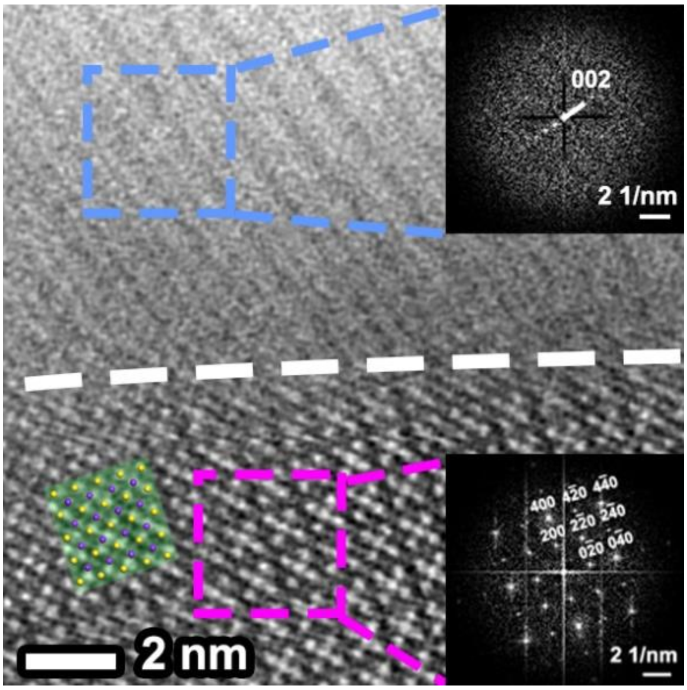

Figure S5. Atomic resolution HAADF-STEM image of MoS_2/FNS interface. The right-top inset shows the fast Fourier transform (FFT) of the selected blue dash box, corresponding to the lattice of MoS_2 (002) planar; the right-bottom inset show the FFT of the pink dash box, containing the FNS (220) and (200) planar. The inset left bottom show the atomic model of FNS, in which the yellow balls represent S atoms while the purple ones stand for Fe/Ni atoms.

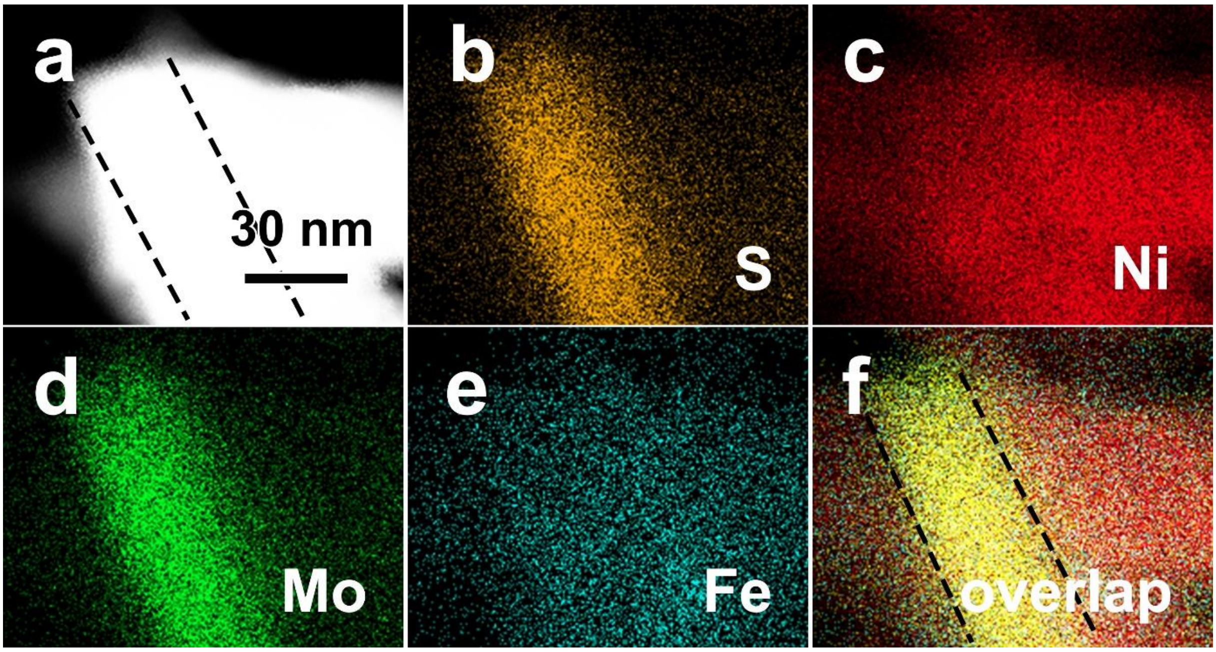

Figure S6. High-resolution EDX-mapping of top view of MoS_2 on FNS. The black dash lines show the interface between MoS_2 and FNS.

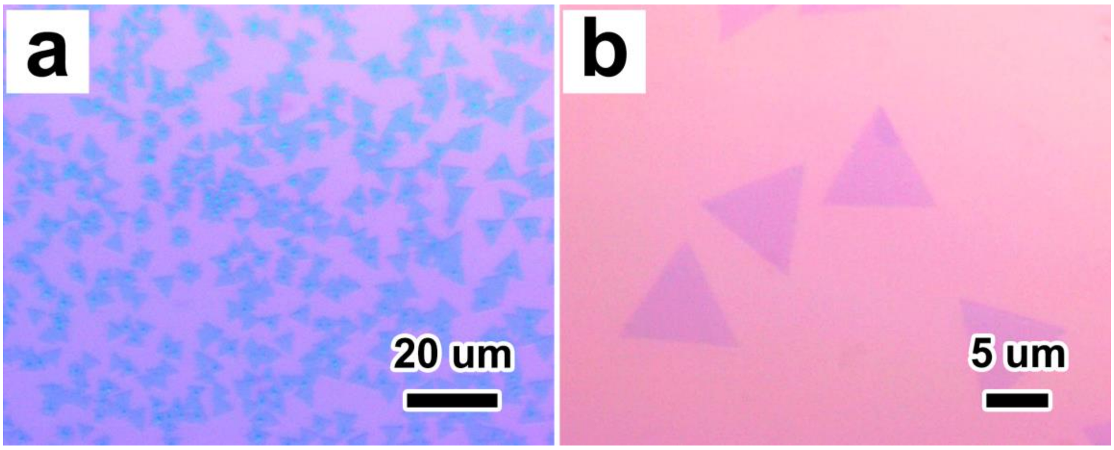

Figure S7. Optical images of MoS_2 grown on SiO_2/Si substrates in a constant flow rate of 50 sccm of N_2 gas at 650^{o}C for 10 min.

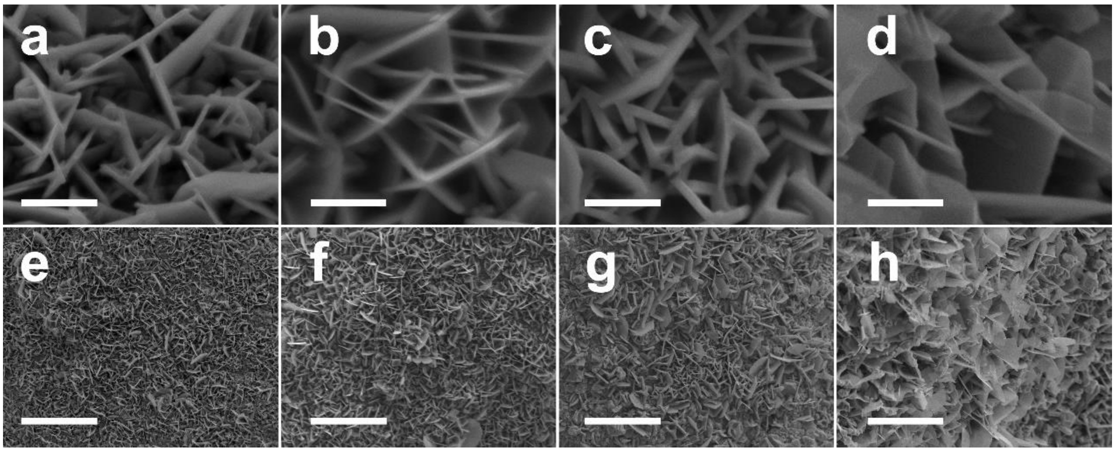

Figure S8. SEM of MoS_2/FNS/FeNi foam with different MoS_2 deposition periods at 650 ^oC in the flow rate of 50 sccm of N_2. (a, e) 10 min, (b, f) 20 min, (c, g) 30 min, (d, h) 60 min. Scale bar: (a-d) 500 nm, (e-h) 5μm.

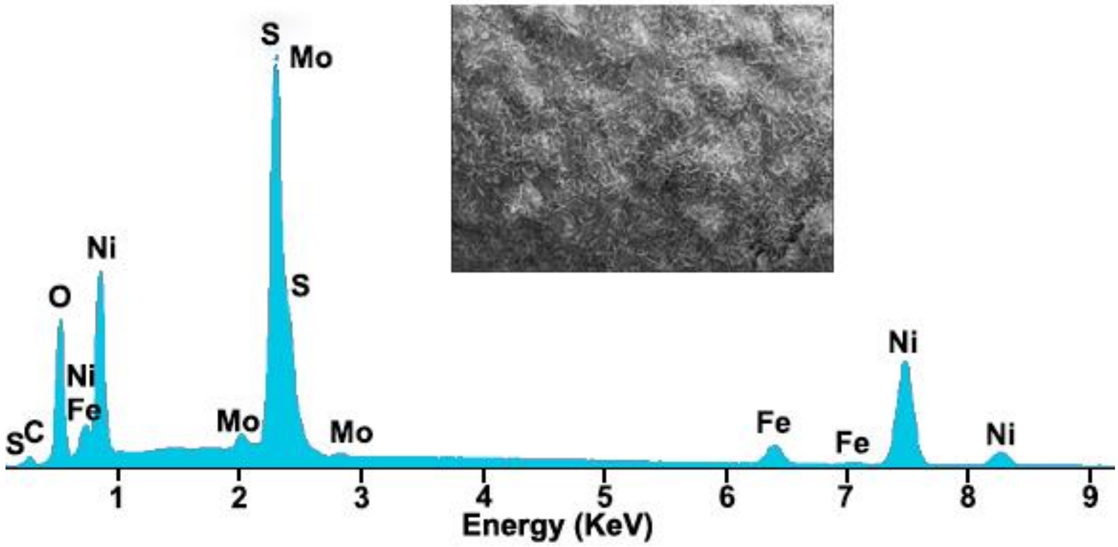

Figure S9. SEM-EDS of MoS_2/FNS/FeNi foam.

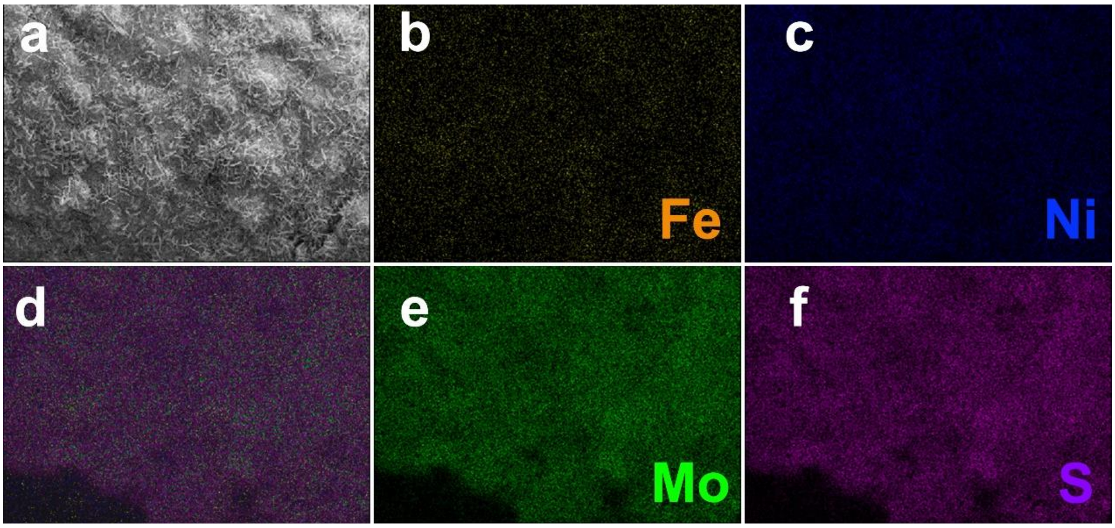

Figure S10. EDX mapping of MoS_2/FNS/FeNi foam. (a) SEM images and corresponding mapping images of elements (b) Fe, (c) Ni, (d) mixed elements of Fe, Ni, Mo and S, (e) Mo and (f) S.

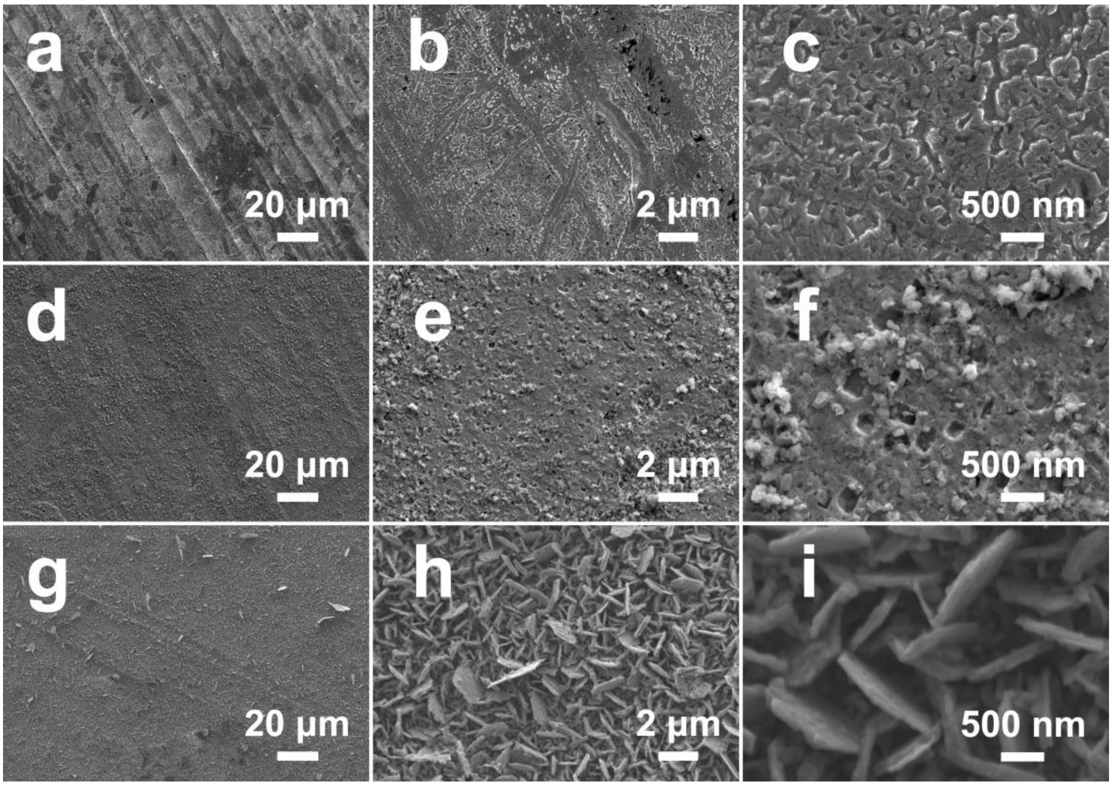

Figure S11. SEM of pure FeNi foil, FNS/FeNi foil and MoS_2/FNS/FeNi foil with different magnifications. (a, b, c) pure FeNi foil, (d, e, f) FNS/FeNi foil, (g, h, i) MoS_2/FNS/FeNi foil.

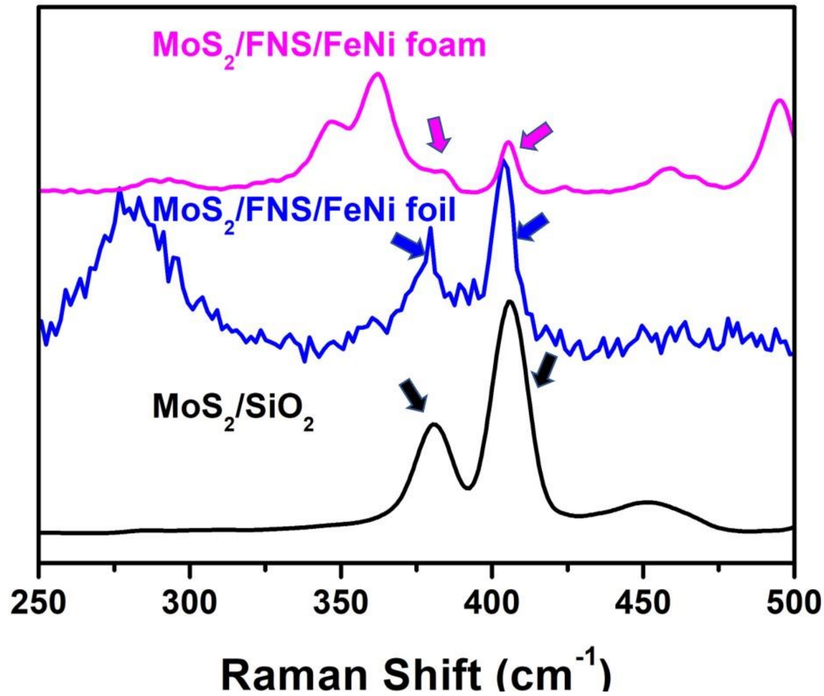

Figure S12. Raman spectroscopy of MoS_2/FNS/FeNi substrates and MoS_2/SiO_2. (The arrows point out the characteristic peaks of MoS_2).

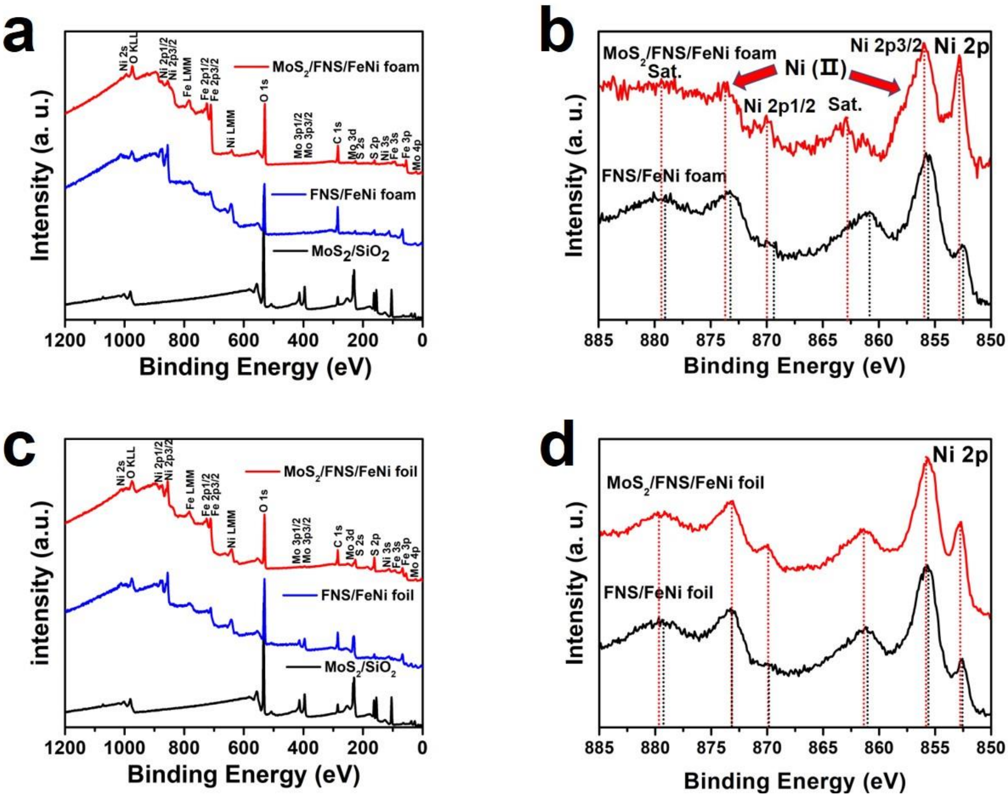

Figure S13. XPS of MoS_2/FNS/FeNi substrates. (a) full spectrum and (b) Ni 2p orbit of MoS_2/FNS/FeNi foam, (c) full spectrum and (d) Ni 2p orbit of MoS_2/FNS/FeNi foil.

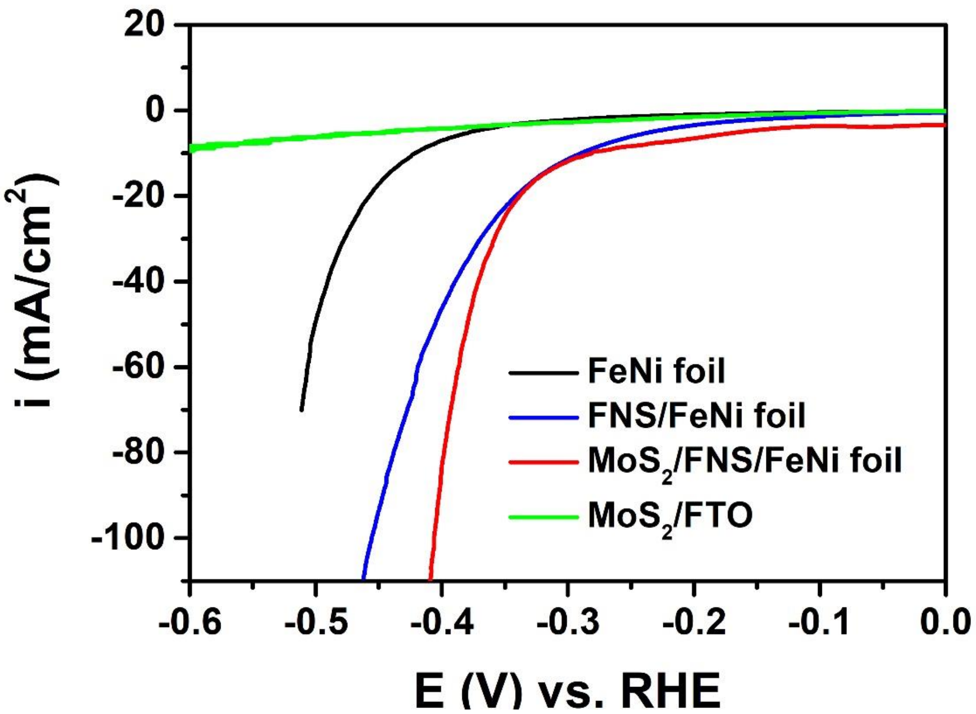

Figure S14. The polarization curves of MoS_2/FNS/FeNi foil, FNS/FeNi foil, FeNi foil and MoS_2/FTO.

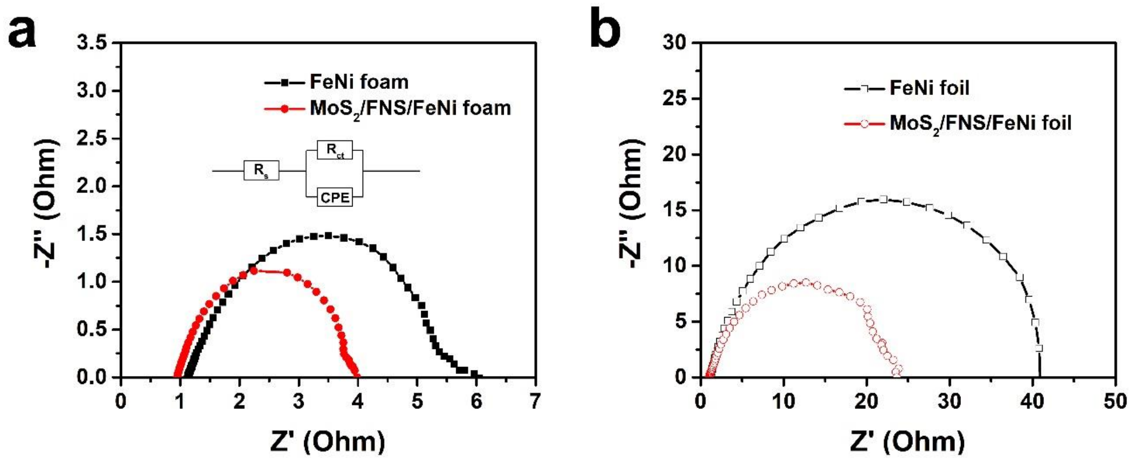

Figure S15. Nyquist plots (overpotential = 250 mV) of MoS_2/FNS/FeNi substrates for HER.

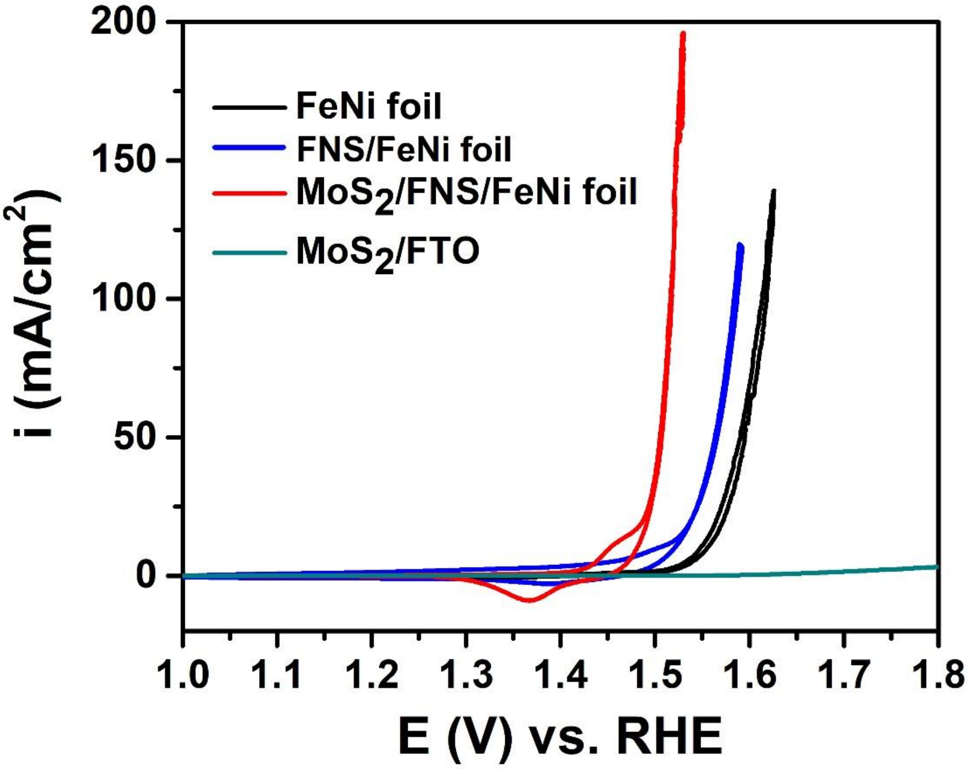

Figure S16. The cyclic voltammograms (CV) of the MoS_2/FNS/FeNi foil, FNS/FeNi foil, FeNi foil and MoS_2/FTO. We analyzed the backward CV curves for OER performances, owing to the oxidation peaks in forwarding scan.

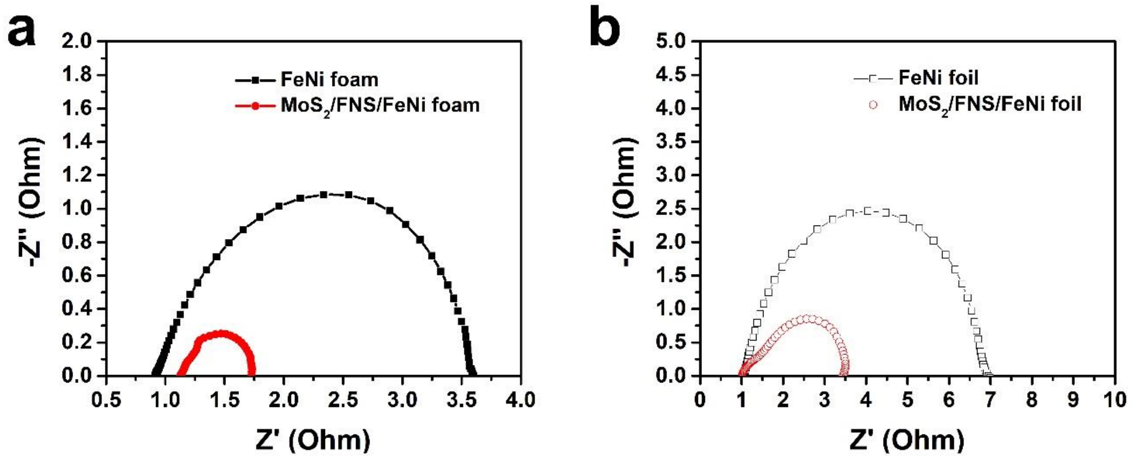

Figure S17. Nyquist plots (overpotential = 250 mV) of MoS_2/FNS/FeNi substrates for OER.

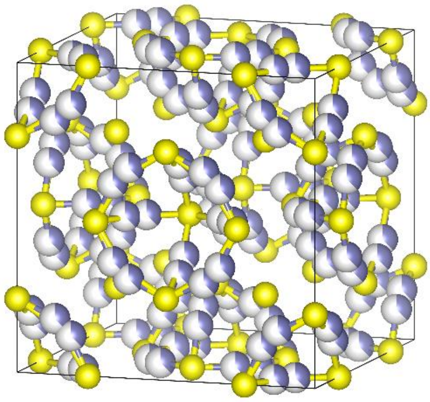

Figure S18. The atomic model of $Fe_5Ni_4S_8$, whose phase prototype belongs to Co_9S_8, that means, there is a chance of 5/9 for Fe and 4/9 for Ni in the position of Co.

Table S1. HER overpotentials at different current density for different samples in this work; mass loading of MoS_2/Pt on FeNi substrates; the specific activity (compared to MoS_2/Pt mass) at an overpotential of η = 250 mV.

Samples	**η (mV) @ 10 mA/cm^2**	**η (mV) @ 20 mA/cm^2**	**η (mV) @ 50 mA/cm^2**	**geometrical area (cm^2)**	**MoS_2/Pt mass loading (mg/cm^2)**	**Specific activity (mA mg^{-1} @ 250 mV)**
MoS_2/FNS/FeNi foam	122	208	265	1.25	0.153	252.7
FNS/FeNi foam	236	283	342	1.25	—	—
FeNi foam	299	352	445	1.25	—	—
MoS_2/FNS/FeNi foil	281	338	380	1.25	0.098	85.5
FNS/FeNi foil	290	341	405	1.25	—	—
FeNi foil	421	457	501	1.25	—	—
MoS_2/FTO	615	—	—	0.89	0.133	15.9
Pt/C/FeNi foam	127	179	235	1.25	0.160	396.6

Table S2. Comparison of the MoS_2/FNS/FeNi substrates to recently reported catalysts for HER. (Catalyst amount is normalized to the geometrical area)

Catalyst	Catalyst amount (mg/cm^2)	Overpotential (vs. RHE) at 10 mA/cm^2 (mV)	Reference
CoFe LDH-F/Ni foam	1.00	166	[4]
CoO_x@CN	0.12	232	[5]
mPF-Co-MoS_2	0.50	156	[6]
MoS_2-P	0.28	251	[7]
Edge-oriented MoS_2 film	—	275	[8]
MoS_2/glassy carbon	—	480	[9]
MoS_2/Graphene/Ni foam	8.09	150	[10]
P-1T-MoS_2	0.14	153	[11]
MoS_2/FNS/FeNi foam	0.15	122	This Work
MoS_2/FNS/FeNi foil	0.10	281	This Work

Table S3. OER overpotentials (mV) at different current density for different samples in this work; mass loading of FNS/IrO_2 on FeNi substrates; the specific activity (compared to FNS & IrO_2 mass) at an overpotential of η = 250 mV.

.

Samples	**η (mV) @ 10 mA/cm^2**	**η (mV) @ 20 mA/cm^2**	**η (mV) @ 50 mA/cm^2**	**Total mass (mg)**	**FNS/IrO_2 mass loading (mg/cm^2)**	**Specific activity (mA mg^{-1} @ 250 mV)**
MoS_2/FNS/FeNi foam	204	218	234	238.6	0.366	565.2
FNS/FeNi foam	265	280	298	227.3	0.605	8.9
FeNi foam	288	305	321	224.2	—	—
MoS_2/FNS/FeNi foil	251	263	277	372.8	0.085	108.9
FNS/FeNi foil	290	308	335	408.6	0.396	4.67
FeNi foil	326	342	365	370.8	—	—
MoS_2/FTO	674	—	—	552.4	—	—
IrO_2/FeNi foam	306	320	334	230.4	0.500	6.9

Table S4. Comparison of the MoS_2/FNS/FeNi substrates to recently reported catalysts for OER

Catalyst	Catalyst amount (mg/cm^2)	Overpotential (vs. RHE) at 10 mA/cm^2 (mV)	Reference
CoO_x@CN	0.12	232	[5]
CoFe LDH-F/Ni foam	1.00	260	[4]
MoS_2/Ni_2S_3	9.70	218	[12]
Co@MoS_2	0.06	270	[13]
CoFe LDHs-Ar	0.20	266	[14]
α-$Ni(OH)_2$	0.20	331	[15]
$FeNi_{4.34}$@FeNi foil	—	283	[16]
NiFeP	—	219	[17]
$Ni_{1/3}Fe_{2/3}$-rGO	0.25	210	[18]
FeNi-rGO LDH	0.25	206	[19]
NiFe-LDH/Ni foam	—	210	[20]
MoS_2/FNS/FeNi foam	0.37	204	This Work
MoS_2/FNS/FeNi foil	0.09	251	This Work

References

[1] G. Kresse, J. Furthmuller, *Phys. Rev. B* **1996**, 54, 11169.

[2] G. Kresse, D. Joubert, *Phys. Rev. B* **1999**, 59, 1758.

[3] P. E. Blochl, *Phys. Rev. B: Condens. Matter* **1994**, 50, 17953.

[4] P. F. Liu, S. Yang, B. Zhang, H. G. Yang, *ACS Appl. Mater. Interfaces* **2016**, 8, 34474.

[5] H. Jin, J. Wang, D. Su, Z. Wei, Z. Pang, Y. Wang, *J. Am. Chem. Soc.* **2015**, 137, 2688.

[6] J. Deng, H. Li, S. Wang, D. Ding, M. Chen, C. Liu, Z. Tian, K. S. Novoselov, C. Ma, D. Deng, X. Bao, *Nat. Commun.* **2017**, 8, 14430.

[7] X. Lu, Y. Lin, H. Dong, W. Dai, X. Chen, X. Qu, X. Zhang, Sci Rep 2017, 7, 42309.

[8] Y. Yang, H. Fei, G. Ruan, C. Xiang, J. M. Tour, *Adv. Mater.* **2014**, 26, 8163.

[9] S. Li, S. Wang, M. M. Salamone, A. W. Robertson, S. Nayak, H. Kim, S. C. E. Tsang, M. Pasta, J. H. Warner, *ACS Catal.* **2016**, 7, 877.

[10] Y. H. Chang, C. T. Lin, T. Y. Chen, C. L. Hsu, Y. H. Lee, W. Zhang, K. H. Wei, L. J. Li, *Adv. Mater.* **2013**, 25, 756.

[11] Y. Yin, J. Han, Y. Zhang, X. Zhang, P. Xu, Q. Yuan, L. Samad, X. Wang, Y. Wang, Z. Zhang, P. Zhang, X. Cao, B. Song, S. Jin, *J. Am. Chem. Soc.* **2016**, 138, 7965.

[12] J. Zhang, T. Wang, D. Pohl, B. Rellinghaus, R. Dong, S. Liu, X. Zhuang, X. Feng, *Angew. Chem. Int. Ed.* **2016**, 55, 6702.

[13] D. Xiong, Q. Zhang, W. Li, J. Li, X. Fu, M. F. Cerqueira, P. Alpuim, L. Liu, *Nanoscale* **2017**, 9, 2711.

[14] Y. Wang, Y. Zhang, Z. Liu, C. Xie, S. Feng, D. Liu, M. Shao, S. Wang, *Angew. Chem. Int. Ed.* **2017**, 56, 5867.

[15] M. Gao, W. Sheng, Z. Zhuang, Q. Fang, S. Gu, J. Jiang, Y. Yan, *J. Am. Chem. Soc.* **2014**, 136, 7077.

[16] U. Y. Qazi, C. Z. Yuan, N. Ullah, Y. F. Jiang, M. Imran, A. Zeb, S. J. Zhao, R. Javaid, A.

W. Xu, *ACS Appl. Mater. Interfaces* **2017**, 9, 28627.

[17]F. Hu, S. Zhu, S. Chen, Y. Li, L. Ma, T. Wu, Y. Zhang, C. Wang, C. Liu, X. Yang, L. Song, X. Yang, Y. Xiong, *Adv. Mater.* **2017**, 29, 1606570.

[18]W. Ma, R. Ma, C. Wang, J. Liang, X. Liu, K. Zhou, T. Sasaki, *ACS Nano* **2015**, 9, 1977.

[19]X. Long, J. Li, S. Xiao, K. Yan, Z. Wang, H. Chen, S. Yang, *Angew. Chem. Int. Ed.* **2014**, 53, 7584.

[20]J. Luo, J.-H. Im, M. T. Mayer, M. Schreier, M. K. Nazeeruddin, N.-G. Park, S. D. Tilley, H. J. Fan, M. Grätzel, *Science* **2014**, 345, 1593.